

# Prospects for High-Precision Pulsar Timing with the New Effelsberg PSRIX Backend

P. Lazarus<sup>1\*</sup>, R. Karuppusamy<sup>1</sup>, E. Graikou<sup>1</sup>, R. N. Caballero<sup>1</sup>,  
D. J. Champion<sup>1</sup>, K. J. Lee<sup>2,1</sup>, J. P. W. Verbiest<sup>3,1</sup>, M. Kramer<sup>1,4</sup>

<sup>1</sup>*Max-Planck-Institut für Radioastronomie, Auf dem Hügel 69, 53121 Bonn, Germany*

<sup>2</sup>*Kavli institute for astronomy and astrophysics, Peking University, Beijing 100871, P.R.China*

<sup>3</sup>*Fakultät für Physik, Universität Bielefeld, Postfach 100131, 33501 Bielefeld, Germany*

<sup>4</sup>*Jodrell Bank Centre for Astrophysics, University of Manchester, Manchester, M13 9PL, United Kingdom*

26 January 2016

## ABSTRACT

The PSRIX backend is the primary pulsar timing instrument of the Effelsberg 100-m radio telescope since early 2011. This new ROACH-based system enables bandwidths up to 500 MHz to be recorded, significantly more than what was possible with its predecessor, the Effelsberg-Berkeley Pulsar Processor (EBPP). We review the first four years of PSRIX timing data for 33 pulsars collected as part of the monthly European Pulsar Timing Array (EPTA) observations. We describe the automated data analysis pipeline, *CoastGuard*, that we developed to reduce these observations. We also introduce *TOASTER*, the EPTA timing database used to store timing results, processing information and observation metadata. Using these new tools, we measure the phase-averaged flux densities at 1.4 GHz of all 33 pulsars. For 7 of these pulsars, our flux density measurements are the first values ever reported. For the other 26 pulsars, we compare our flux density measurements with previously published values. By comparing PSRIX data with EBPP data, we find an improvement of  $\sim 2$ – $5$  times in signal-to-noise ratio achievable, which translates to an increase of  $\sim 2$ – $5$  times in pulse time-of-arrival (TOA) precision. We show that such an improvement in TOA precision will improve the sensitivity to the stochastic gravitational wave background. Finally, we showcase the flexibility of the new PSRIX backend by observing several millisecond-period pulsars (MSPs) at 5 and 9 GHz. Motivated by our detections, we discuss the potential for complementing existing pulsar timing array data sets with MSP monitoring campaigns at these frequencies.

**Key words:** pulsars: general – stars: neutron – gravitational waves

## 1 INTRODUCTION

Pulsars are extremely useful tools for studying various fields of astrophysics. Many important results are the product of regular timing campaigns that are used to determine models of pulsars’ rotation capable of accounting for every rotation of the star. High-precision timing observations of millisecond-period pulsars (MSPs) have proven to have a large number of diverse applications, such as testing of relativistic gravity (e.g. Kramer et al. 2006), constraining the equation-of-state of ultra-dense matter (e.g. Demorest et al. 2010), and studying binary stellar evolution (e.g. Freire et al. 2011). In general, studies of radio pulsars

have also been used to probe the interstellar medium (e.g. Bhat et al. 1998; Berkhuijsen & Müller 2008; Eatough et al. 2013). Furthermore, collections of MSPs are being observed regularly as part of so-called pulsar timing array (PTA) projects, which have the ultimate goal of detecting low-frequency gravitational waves, possibly arising from the cosmic population of super-massive black-hole binaries (e.g. Sesana 2013) or from cosmic strings (e.g. Sanidas et al. 2012).

To maximise the scientific potential of pulsar timing observations, high signal-to-noise ratio ( $S/N$ ) observations are required to determine pulse times of arrival (TOAs) precisely. Given a telescope, the  $S/N$  can be improved either by increasing the integration time, which is limited by the total available telescope time and the number of pulsars to ob-

\* E-mail: plazarus@mpifr-bonn.mpg.de

serve, or by using more sensitive and/or wider bandwidth receivers. In order to fully leverage wider bandwidths, instruments capable of processing the increased frequency range must be used.

The Effelsberg-Berkeley Pulsar Processor (EBPP) coherent dedispersion backend (Backer et al. 1997) has been running since 1995. Its long, uniform data sets for some MSPs have enabled unique studies. For example, Shao et al. (2013) used EBPP data to constrain profile variations in MSPs, and thus improve limits on the violation of local Lorentz invariance of gravity by several orders of magnitude relative to previously published limits (see Will 1993, and references therein). The EBPP data set has also been a key component of several European Pulsar Timing Array (EPTA) projects, such as characterising the noise properties of MSPs (Caballero et al. 2015), constraining the low-frequency gravitational wave background (GWB; Lentati et al. 2015), and searching for single sources of gravitational waves (GWs; Babak et al., accepted).

The EBPP is beginning to show its age. For instance, the EBPP bandwidth is limited to only  $\sim 64$ – $128$  MHz, depending on the integrated Galactic electron content along the line-of-sight to the pulsar (i.e. the pulsar’s dispersion measure, DM), whereas most current receiver systems operating in the 1–3 GHz band can simultaneously observe bandwidths of 200–800 MHz (e.g. the Greenbank Ultimate Pulsar Processing Instrument – GUPPI – used at the Green Bank Telescope, and its clones PUPPI and NUPPI at the Arecibo and Nançay observatories, respectively Ford et al. 2010), and in the case of the Ultra-Broadband (UBB) receiver at Effelsberg,  $\sim 2600$  MHz. Furthermore, the EBPP hardware is becoming increasingly unreliable, and replacement parts are increasingly difficult to come by.

For these reasons, the EBPP backend was replaced as the main data recorder for pulsar timing observations at Effelsberg by the PSRIX backend in 2011 March. PSRIX is built around a Reconfigurable Open Architecture Computing Hardware (ROACH) system, a programmable platform designed by the Collaboration for Astronomy Signal Processing and Electronics Research (CASPER).<sup>1</sup> The EBPP is still run in parallel with PSRIX whenever possible.

PSRIX was originally designed as part of the Large European Array for Pulsars (LEAP) project (Bassa et al. 2015), which has the objective of coherently combining signals from the five largest European radio telescopes.<sup>2</sup> To meet this goal, the primary mode of operation of PSRIX is to record baseband data, however, additional modes were implemented to record coherently dedispersed profiles folded in real-time and coherently dedispersed single pulses. PSRIX’s coherent-dedispersion modes support bandwidths up to 500 MHz and are flexible enough to observe at different frequencies, taking advantage of Effelsberg’s many receivers. Technical details of the backend design and the implementation its various modes of operation will be described in a future paper.

Thanks to the increased bandwidth and more robust

design of PSRIX compared to the EBPP, the timing campaigns undertaken at Effelsberg using PSRIX are producing data of superior quality, thus enabling even higher-precision timing studies than previously possible. Moreover, PSRIX may further improve the prospects of high-precision timing at Effelsberg by making it is possible to conduct timing observations of MSPs at 5 GHz and higher, helping to mitigate noise arising from variations of the ISM along the line of sight towards the pulsar, a serious impediment to searches for GWs with PTAs.

The EPTA has previously incorporated the  $\sim 17$ -year-long EBPP data set into its timing analyses and GW searches (e.g. Desvignes et al., submitted; Janssen et al. 2008; Lazaridis et al. 2009, 2011; Lentati et al. 2015). Here we describe the PSRIX data and its analysis, which will be included in future EPTA projects and be shared with the International Pulsar Timing Array (IPTA) collaboration (Verbiest et al., submitted).

In addition to the monthly observing sessions of many binary pulsars and MSPs, several pulsars have been the target of dedicated observing campaigns with PSRIX over the past four years. In particular, PSRIX data were included in the IPTA effort to observe PSR J1713+0747 continuously for 24 hours using the largest radio telescopes around the Earth (Dolch et al. 2014). Also, PSR J0348+0432, a  $2-M_{\odot}$  pulsar in a  $\sim 2.5$  hr relativistic binary with a white-dwarf companion (Lynch et al. 2013; Antoniadis et al. 2013), has been regularly observed for full orbits using PSRIX. Several full-orbit observing campaigns of PSR J1518+4904, a 41-ms pulsar in an 8.6-day double-neutron-star binary, have been conducted with PSRIX to precisely measure the mass of the pulsar and its companion (Janssen et al., in prep.).

The remainder of this paper is organised as follows. Section 2 describes the monthly EPTA observations undertaken with the Effelsberg telescope using PSRIX. The analysis of these observations is detailed in § 3, and includes an overview of the automated data reduction suite **CoastGuard**, as well as the timing database **TOASTER**. Flux density measurements for 33 pulsars at 1.4 GHz and a comparison between PSRIX and the old EBPP backends are presented in § 4, as are the results of observations at 5 and 9 GHz. The results are discussed in § 5 and the paper is finally summarised in § 6.

## 2 OBSERVATIONS

Every month, the Effelsberg radio telescope is used to observe bright, stable MSPs as part of the EPTA project. These observations are conducted with PSRIX in its coherent-dedispersion real-time folding mode, evenly dividing the pulse profiles into 1024 phase bins. Each session typically consists of observations at both 1.4 and 2.6 GHz (wavelengths of 21 and 11 cm, respectively). The 1.4-GHz observations use either the central feed of the 7-beam receiver (called “P217mm”) or the single-feed 1.4 GHz receiver (“P200mm”).<sup>3</sup> Both of these 1.4-GHz receivers are situated in the primary focus of the Effelsberg telescope. Only one of the 1.4-GHz receivers is installed for any given observing

<sup>1</sup> <https://casper.berkeley.edu/>

<sup>2</sup> Specifically, the Lovell Telescope, the Westerbork Synthesis Radio Telescope, the Nançay Telescope, the Sardinia Radio Telescope, and Effelsberg.

<sup>3</sup> <http://www.mpifr-bonn.mpg.de/effelsberg/astronomen>

session. We use whichever receiver is available. The 2.6-GHz observations are done with the “S110mm” secondary-focus receiver. PSRIX is used to record a 200-MHz band, which is divided into eight 25-MHz sub-bands. In the case of P200mm and S110mm observations, this exceeds the available bandwidths of 140 MHz and 80 MHz, respectively. See Table 1 for details of the observing set-ups used. All of the receivers used in this work have circularly polarised feeds.

Whenever possible, we record data with the EBPP coherent-dedispersion pulsar timing backend in parallel with PSRIX. This allows for a more accurate determination of the time offset between the two instruments. We have also used these simultaneous observations to characterise the improvement of PSRIX over the EBPP (see § 4.3).

Our monthly EPTA observing sessions typically consist of 24 hours at 1.4 GHz and 12–24 hours at 2.6 GHz. Each observing session includes pulsar observations of ~30–60 min in duration. Polarisation calibration scans are conducted prior to each pulsar observation and each consist of a 2-min integration of the receiver noise diode offset by  $0.5^\circ$  from the pulsar position. The diode is pulsed with a 1-s repetition rate and a 50% duty cycle.

Since 2013, at 1.4 GHz, we also performed on- and off-source scans of a radio source with a stable, well-known flux density, usually 3C 218 (i.e. Hydra A). These flux calibration observations use the noise diode as described above.

Every month, we observe ~45 pulsars at 1.4 GHz and ~20 pulsars at 2.6 GHz. Pulsars that are never, or rarely, detected at 2.6 GHz during a 6–12 month probationary period are dropped from the regular observing schedule. Here we focus on the data sets of 33 MSPs and binary pulsars acquired between 2011 and 2015. Tables 2 and 3 show a summary of our 1.4 and 2.6 GHz observations of these pulsars, respectively.

As we will discuss in § 5.2, since ISM effects weaken with increasing radio frequency, high-frequency observations of pulsars may be extremely useful to avoid and mitigate the effects of variability in the interstellar medium (ISM), which limit the sensitivity of attempts at detecting GWs with pulsars. In 2015 January, we conducted observations of 12 MSPs at 5 GHz (6 cm) using the “S60mm” secondary-focus receiver with the aim of assessing their utility to the PTAs. We used PSRIX in its 500-MHz coherent-dedispersion real-time folding mode for these 5 observations. We also observed four of these pulsars at 9 GHz (3.6 cm) with the “S36mm”, also a secondary-focus receiver, again with 500 MHz of bandwidth. Our high-frequency observations are listed in Table 4. We selected the pulsars for these exploratory high-frequency observations based on their 1.4 and 2.6 GHz detection significances, which we scaled to higher frequencies using the radiometer equation, the receiver performance, and published spectral indices.<sup>4</sup> Specifically, we required an estimated  $S/N \gtrsim 10$  for a 30-min observation when selecting pulsars for the preliminary 5 and 9-GHz observations reported here. High-frequency observations of other (fainter) MSPs are being conducted and will be reported elsewhere.

### 3 DATA ANALYSIS

#### 3.1 CoastGuard: An Automated Timing Data Reduction Pipeline

We developed an automated pipeline, *CoastGuard*,<sup>5</sup> to reduce PSRIX data. *CoastGuard* is written in python and is largely built around programs from the *psrchive* package<sup>6</sup> (Hotan et al. 2004), using its python wrappers to read PSRIX data files, which are *psrchive*-compatible. *CoastGuard* contains components that are sufficiently general for use with *psrchive*-compatible data files from other observing systems despite that it was primarily designed for Effelsberg PSRIX data. In particular, the radio frequency interference (RFI) removal algorithm described below has been applied to data from the Parkes Telescope (Ng et al. 2014) and has also been adopted by the LOFAR pulsar timing data reduction pipeline (Konradiev et al. 2015).

*CoastGuard* contains considerable error checking, logging, logistics, and control logic required to automate large portions of the pipeline, which is marshalled by a control script and a MySQL database.

In its coherent-dedispersion real-time folding mode the PSRIX backend writes data files every 10 s for each 25-MHz sub-band. These fragments are then grouped together and combined using *psradd*. At this stage, the data are realigned using an up-to-date pulsar ephemeris, if necessary, and 12.5% of the channels at the edge of each sub-band are zero-weighted to reduce the effect of aliasing.

Next, the metadata stored in these consolidated files are cross-checked against telescope observing logs and all discrepancies are corrected. This is primarily to repair issues with the observation metadata that were common during the commissioning of PSRIX. These issues have since been resolved.

The data files are then cleaned of RFI. In the pipeline, our cleaning process excludes RFI by setting the weights of individual profiles to zero. That is, the data from RFI-affected sub-integration/channel combinations are ignored in the rest of the analysis without altering the data values. Therefore, it is possible to reverse the automated RFI masking.

*CoastGuard*’s RFI-excision script, *clean.py*, includes four distinct algorithms that can be chained together to clean corrupted data. Each algorithm has several parameters that can be used to optimise its performance. In our automated data analysis, we use two of the four available cleaning algorithms, namely *rcvrstd* and *surgical*. The other two algorithms, *bandwagon* and *hotbins*, are occasionally applied manually to observations requiring special attention. Our standard RFI excision algorithm proceeds as follows:

First, *clean.py*’s *rcvrstd* algorithm is used to zero-weight frequency channels beyond the receiver response and channels falling within a list of receiver-dependent bad frequency intervals.

Second, the *surgical* algorithm is used to find profiles corrupted by RFI in the folded data cube. To avoid being biased by the presence of the pulsar signal, the ampli-

<sup>4</sup> For pulsars without spectral indices available in the literature, we used a spectral index of  $\alpha = -2$  for our estimates.

<sup>5</sup> Available at [https://github.com/plazar/coast\\_guard](https://github.com/plazar/coast_guard)

<sup>6</sup> <http://psrchive.sourceforge.net/>

tude and phase of the integrated pulse profile is fit using a least-squares algorithm to individual profiles containing a significant detection and the difference is computed. It is these pulsar-free residuals that are treated in the remainder of the algorithm. Next, RFI-contaminated data are identified with a set of four metrics, which are computed for each sub-integration/channel pair (i.e. each total-intensity profile stored in the data file). These metrics are: 1) the standard deviation, 2) the mean, 3) the range, and 4) the maximum amplitude of the Fourier transform of the mean-subtracted residuals. These four metrics were selected due to their sensitivity to the RFI signals present in Effelsberg data, which include, but are not limited to: excess noise, occasional data drop-outs, and infrequently, rapid (sub-ms) periodic bursts. For each metric, a  $N_{\text{sub}} \times N_{\text{chan}}$ -sized matrix of values is produced. Trends in the rows and columns of these matrices are removed by subtracting piece-wise quadratic functions that were fit to the data. The subtraction of these trends account for slow variations in time, as well as the shape of the bandpass. These rescaled matrices are then searched for outliers, which are defined as being  $>5\sigma$  from the median of either their sub-integration or channel. Finally, profiles that are identified as an outlier by at least two of the four metrics are zero-weighted.

The `bandwagon` algorithm completely removes sub-integrations and channels that already have a sufficiently large fraction of data masked, and the `hotbins` algorithm replaces outlier off-pulse profile phase-bins with locally sourced noise.<sup>7</sup> Neither of these two algorithms are part of our standard automated data reduction.

Once the observations are cleaned, they are reviewed before proceeding with the rest of the automated analysis. This is to identify observations that still need to be cleaned manually. In practice, only a small fraction of observations require additional RFI zapping. This quality-control stage also provides an opportunity to identify observations where the pulsar is not detected or where the data are contaminated by RFI beyond repair. Observations falling into these two categories do not continue further in the data reduction process.

The above data reduction process (combine, correct, clean, quality control) is also applied to polarisation calibration scans of the noise diode. The cleaned and vetted calibration scans are fully time-integrated, and then loaded into the appropriate `psrchive` `pac`-compatible “database” files. The pipeline maintains one calibration database file for each pulsar.

Polarisation calibration of the cleaned pulsar data files is performed with `psrchive`’s `pac` program,<sup>8</sup> using its “SingleAxis” algorithm, which appropriately adjusts the relative gain and phase difference of the two polarisation channels by applying the technique of Britton (2000). These calibrated observations are manually reviewed a second time to verify that no artifacts have been introduced.

Flux calibration has not been incorporated into the automated data analysis pipeline. Nevertheless, we have manually performed flux calibration wherever possible. In our analysis we used `psrchive`’s `fluxcal` and `pac` programs.

`fluxcal` compares the power levels of on- and off-source observations of a standard candle target to determine the system equivalent flux density over the observing band. This information is used to determine the flux density scale of the polarisation-calibrated pulsar observations.

For this paper we refolded all data with up-to-date ephemerides.

### 3.2 TOASTER: The TOAs Tracker Database

We have developed a python package, TOAS TrackER (TOASTER),<sup>9</sup> for computing and storing TOAs in a fully described and reproducible way. At its core, TOASTER consists of an SQL database and full-featured python toolkit for reliably interacting with the data and database.

Beyond simply storing TOA information, TOASTER’s database also records information about telescopes and observing systems, observation information (e.g. frequency, epoch, integration time, the ephemeris used for folding), the standard profile used to determine each TOA, as well as version numbers of relevant software, such as `psrchive` and `TEMPO2` (Hobbs et al. 2006).

Once the database is populated, TOASTER can also launch TOA generation processes that use a variety of “manipulators” to prepare the data prior to automatically computing TOAs using standard `psrchive` tools. The most basic manipulator fully integrates data in frequency and time. However, more sophisticated manipulations can be included to adjust the data according to an updated, possibly time-varying DM, integrate a fixed number of pulses or variable number of pulses depending on the resulting  $S/N$ . Manipulators can also be used to scale the measured profiles to have uniform off-pulse variance, as was done by (Arzoumanian et al. 2015). Typically these types of manipulations are included in the data reduction pipelines that prepare observations prior to determining TOAs. By performing these data reduction steps in TOASTER, the details of the manipulations performed on the data and the resulting TOAs are logged in the database, making it easy to store the resulting TOAs, as well as systematically compare the effect of different manipulations on the eventual timing analysis. Furthermore, the TOASTER database includes a reference to the template used to compute each TOAs. The end result is a completely described and reproducible TOA-generation procedure. This makes TOASTER a useful tool for high-precision timing projects like the EPTA and IPTA that are constantly adding new data, as well as developing new data reduction algorithms.

The TOASTER toolkit scripts can be used to easily query the information stored in its database. For example, TOASTER provides scripts to list and summarise the TOAs in the database. These scripts can also be used to generate TOA files in multiple formats, including a `TEMPO2` format that includes all the annotations (“TOA flags”) requested by the IPTA.

TOASTER can be used to load TOAs directly into the database (i.e. without information concerning the observations, templates, etc.). This feature is useful for including

<sup>7</sup> Because the `hotbins` algorithm replaces data, it is irreversible.

<sup>8</sup> <http://psrchive.sourceforge.net/manuals/pac/>

<sup>9</sup> TOASTER and its documentation are publicly available at <https://github.com/plazar/toaster>

previously computed, and finalised, data sets, such as the EPTA legacy TOAs (Desvignes et al., submitted).

We set up the **TOASTER** software and database to manage the reduced (i.e. cleaned and calibrated) PSRIX data, which are automatically loaded into the **TOASTER** database by the data reduction pipeline described in § 3.1.

## 4 RESULTS

Over the past four years, we have collected timing data on 45 pulsars at 1.4 and 2.6 GHz using the PSRIX backend with the 100-m Effelsberg radio telescope. Here we report on a selection of 33 pulsars. Most of these pulsars have been monitored monthly in both bands for the entire 4-year period. An overview of our 1.4 and 2.6 GHz observations can be found in Tables 2 and 3, respectively.

### 4.1 Flux Density Measurements

We measured flux densities for all 33 pulsars at 1.4 GHz. For each pulsar, we report the mean flux density,  $\langle S \rangle$ , and the median flux density,  $S_{\text{med.}}$ , to account for observed modulation due to interstellar scintillation. We estimate the precision of the mean flux densities as the standard error on the mean, that is,

$$\delta \langle S \rangle = \sigma_S / \sqrt{N_{\text{cal.}}}, \quad (1)$$

where  $\sigma_S$  is the standard deviations of the individual flux measurements and  $N_{\text{cal.}}$  is the number of calibrated observations.

The flux densities we measure are reported in Table 2, along with previously measured values at 1.4 GHz. Seven of the pulsars we report flux densities for do not have previously published measurements, and three other pulsars have previously published measurements that were not calibrated against observations of standard candle sources. Most of the rest of our flux density measurements are consistent with previously reported values (see Fig. 1). Inconsistencies may arise from scintillation, which impacts both the observed flux density as well as the apparent uncertainty. The effect of scintillation is most apparent when only a small number of observations are used to estimate the flux density and is further exacerbated when observations make use of short integrations and/or small bandwidths.

Data from 2013 Nov. to 2014 Aug. could not be calibrated due to saturation and/or non-linearities in the data resulting from insufficient attenuation of the telescope signal. Fortunately, this was only an issue when observing extremely strong sources (e.g. flux calibrators with the noise diode). We find no anomalies in the observed pulse profiles, allowing these observation from late-2013 to mid-2014 to be used for timing.

### 4.2 Clock Stability

The PSRIX system suffered four clock offsets over its first four years of operation. The first offset occurred between 2012 Oct. 27 and Nov. 10, and was due to switching clock sources without measuring the phase difference between their signals. The second offset, which occurred on 2013 July 27, was caused by cutting the power to the clock

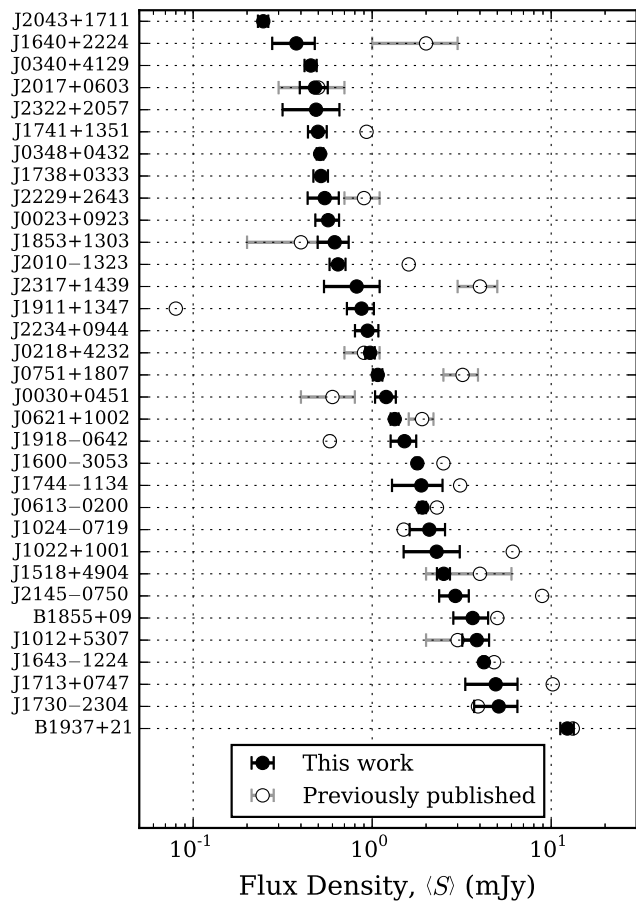


**Figure 1.** Measured 1.4 GHz flux densities of 33 pulsars estimated from averaging over multiple PSRIX observations (filled circles). The uncertainties are estimated as the standard error on the mean (see Eq. 1). Additional details of the calibration process can be found in §§ 3 and 4.1. The previously published flux densities (unfilled circles) do not all have properly measured uncertainties. See Table 2 for notes and references.

signal generator and not re-syncing the phase of the signal after the system was restarted. The third offset was deliberately introduced on 2014 Mar. 4 when the clock signal was synchronised to the original clock phase. Finally, the fourth offset on 2014 Nov. 20 was also deliberately introduced by installing a new clock signal generator.

The first two clock offsets were initially measured by fitting timing data for the orbital phase of PSR J0348+0432. These measurements were sufficiently precise to determine the offsets to within one phase rotation of PSR J0348+0432 ( $P \simeq 39$  ms), allowing the values to be further refined by fitting arbitrary time offsets (“JUMPs”) to the timing residuals of PSR J0348+0432 and then with PSR J1744–1134 ( $P \simeq 4.1$  ms). The final values of the clock offsets have been measured by fitting JUMPs individually to the timing data of four pulsars, namely PSRs J0613–0200, J1643–1224, J1713+0747, and J1744–1134. These were selected on the basis of being of the most precisely timed pulsars in the PSRIX data set. The JUMPs were fit simultaneously with pulsar parameters and noise models using **TempoNest**

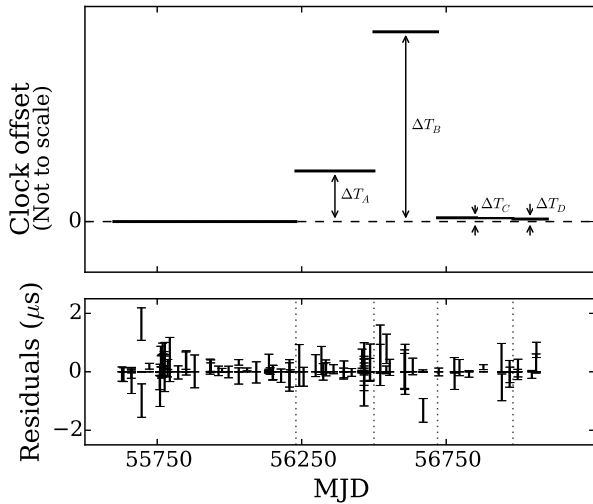


**Figure 2.** *Top* – A schematic of the four clock offsets suffered by the PSRIX system. The offset values are:  $\Delta T_A = 97.2851(6)$  ms,  $\Delta T_B = 409.2691(8)$  ms,  $\Delta T_C = 0.000612(1)$  ms, and  $\Delta T_D = 0.000127(1)$  ms. Offsets *A* and *B* are larger than the spin periods of the pulsars reported here ( $P \sim 1\text{--}50$  ms), thus resulting in phase ambiguities and different apparent offsets in residuals for different pulsars. See § 4.2 for the origins of the clock offsets and how their magnitudes were determined.

*Bottom* – Timing residuals from PSRIX observations at 1.4 GHz of PSR J1713+0747 after accounting for the clock offsets, showing that no significant offsets remain.

(Lentati et al. 2014). The resulting JUMP values, all of which were measured relative to the original clock signal, were averaged together resulting in measurements of  $\Delta T_A = 97.2851(6)$  ms and  $\Delta T_B = 409.2691(8)$  ms. These measurements have been confirmed with data from LEAP by measuring and comparing the phase delays between the signals of simultaneous observations with several European radio telescopes before and after the epochs of the PSRIX clock offsets (see Bassa et al. 2015, for an overview of the project).<sup>10</sup> The third and fourth offsets were directly measured at the telescope by comparing clock signals with an oscilloscope. The results are high-precision measurements of  $\Delta T_C = 0.000612(1)$  ms and  $\Delta T_D = 0.000127(1)$  ms, which are consistent with offset values derived from fitting JUMPs to pulsar timing data.

A schematic of the PSRIX clock offsets is shown in Fig. 2. The timing residuals of PSR J1713+0747 after the JUMPs are removed show no evidence of the clock offsets, as shown in the bottom panel of Fig. 2. Similarly, the residuals of all other pulsars are also free of the effect of the clock offsets after applying the offsets listed above.

Note that the EBPP uses an independent reference clock, and thus was not affected by any of the four offsets seen in the PSRIX data.

<sup>10</sup> The precision of the LEAP-based measurements is expected to surpass what is possible with timing-based JUMP measurements. However, the uncertainties of the LEAP-based measurements are not yet well determined, so here we report the values and uncertainties derived from the more standard and conservative JUMP measurements.

### 4.3 Comparison With the EBPP Backend

We have compared the  $S/N$  derived from data recorded simultaneously with PSRIX and the old EBPP backend (see Fig 3). In particular, we used multiple observations of four MSPs that are best and most frequently timed with PSRIX, PSRs J0613–0200, J1643–1224, J1713+0747, and J1744–1134. We have found that PSRIX provides significantly stronger detections, roughly 2–5 times higher  $S/N$ , than the simultaneously recorded EBPP data. A similar comparison of TOA uncertainties derived for simultaneous PSRIX and EBPP data also shows improvements of a factor of 2–5.

There are several reasons why PSRIX outperforms the EBPP:

- 1) The 200-MHz bandwidth of PSRIX is considerably larger than the EBPP’s usable bandwidth ( $\sim 40\text{--}50$  MHz for most pulsars, and  $\sim 95$  MHz for pulsars with  $DM \lesssim 10$  pc cm<sup>-3</sup>). A comparison of the observing bands from both backends is shown in Fig. 4. PSRIX’s larger bandwidth allows more signal to be integrated, reducing radiometer noise, and also increases the chance of observing constructive scintels.
- 2) The PSRIX data are recorded with 8 bits, making them even more resilient in the presence of strong RFI than the EBPP with its 4-bit data.
- 3) The 10-s sub-integrations of PSRIX are much shorter than the 2-min sub-integrations of the EBPP. Thus, the expense of removing impulsive RFI is diminished. Also, the shorter sub-integrations make re-aligning the pulse profiles with an updated timing model more accurate.
- 4) PSRIX is a more robust instrument than the EBPP. This is especially true now that the latter is nearly 20 years old, and hardware and networking issues occasionally preclude it of recording data. In these instances, data files are cut short, or not written at all.

The increase in bandwidth of PSRIX over the EBPP is even more apparent when full polarisation information is recorded. Polarisation observations with the EBPP are limited to only 28 MHz, whereas with PSRIX full polarisation information can be recorded for up to 500 MHz of bandwidth. Moreover, because recording polarisation information required the EBPP to be set up in a special mode prior to commencing observations, it is much less flexible than PSRIX, which always provides full Stokes parameters for timing-mode observations.

In addition to investigating individual observations, we also examined the timing data of several pulsars to compare the timing stability achievable with PSRIX vs. the EBPP. Depending on the pulsar, we found the weighted root-mean-square (RMS) of the PSRIX timing residuals is a factor of  $\sim 1.3\text{--}3$  times better than that of the EBPP over the same time interval. In our analysis, we whitened the timing residuals with three frequency derivatives and two DM derivatives to not be biased by the effects of pulsar spin noise and DM variations.<sup>11</sup> We also removed the four clock offsets affecting PSRIX data mentioned in § 4.2. The smallest improvement factor we found ( $1.3\times$ ) was for PSR J1744–1134. This is because the pulsar’s particularly low DM of  $3.1$  pc cm<sup>-3</sup> made

<sup>11</sup> The timing residuals from PSRIX and the EBPP closely trace the residuals from other EPTA telescopes, so we are confident that the systematic trends we are removing are not instrumental.

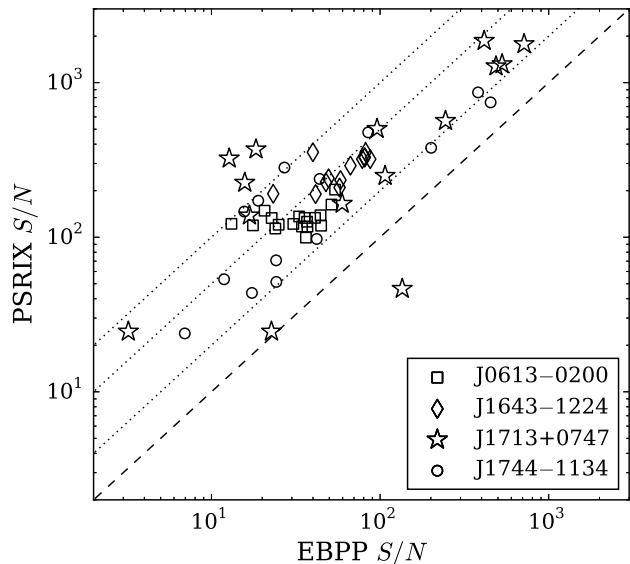


**Figure 3.** Comparison of  $S/N$  for simultaneous observations with the PSRIX and EBPP backends. Equal  $S/N$  is shown with the dashed line. The dotted lines represent 2 $\times$ , 5 $\times$ , and 10 $\times$  improvements. The one observation of PSR J1713+0747 where the  $S/N$  is larger in the EBPP observation is due to there being a single scintillation maximum within the 200-MHz PSRIX band that falls inside the smaller EBPP observing window. Note that we did not weight the frequency channels by  $S/N$  when integrating the band.

it possible for the EBPP to coherently dedisperse  $\sim 95$  MHz of usable bandwidth.

Despite PSRIX providing better detections than the EBPP, we still observe with both backends in parallel whenever possible, to extend the latter’s nearly 20-year long data set.

#### 4.4 High-Frequency Observations

Our 5 and 9-GHz observations of 12 EPTA pulsars all resulted in detections. The integrated pulse profiles from individual high-frequency observations are shown in Fig. 5. PSRs J1012+5307, J1713+0747, B1937+21 were observed twice at 5 GHz, and PSR J2145–0750 was observed twice each 5 and 9 GHz. Details of the 5 and 9-GHz observations presented in Table 4.

To flux calibrate our observations, we observed 3C 48 at both 5 and 9 GHz on 2015 Jan. 7 and again on 2015 Jan. 24. These observations were used to derive calibrated flux densities of our observations at these frequencies. We observed the pulsars to have flux densities ranging from 0.2 to 1.5 mJy at 5 GHz, and from 0.2 to 0.3 mJy at 9 GHz (see Table 4). We found some variation in the measured flux densities of the pulsars observed multiple times. However, these variations are consistent with amplitude modulations expected from weak scintillation at these frequencies (e.g. Lorimer & Kramer 2004).

For each of our high-frequency observations, we computed TOA uncertainties using an analytic template, which was generated by fitting von Mises-shaped pulse components to the summed profile. TOA uncertainties we determined

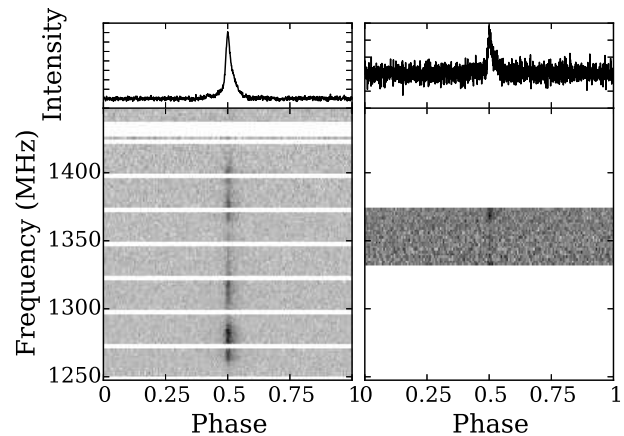


**Figure 4.** *Left* – The integrated pulse profile and frequency vs. phase plot for a 28-min observation with PSRIX of PSR J1713+0747 on 2013 Jan 6. This detection has a  $S/N = 225$  thanks to its 200 MHz bandwidth. The frequency channels missing due to interference and roll-off at the edges of the sub-bands are removed (see §3).

*Right* – The integrated pulse profile and frequency vs. phase plot for the same observation of PSR J1713+0747 using data from EBPP, which was recording in parallel. The EBPP provides a significantly weaker detection with  $S/N = 20$ , owing to its limited  $\sim 40$  MHz bandwidth.

range from 0.1 to 7.5  $\mu$ s at 5 GHz and from 5 to 30  $\mu$ s at 9 GHz (see Table 4).

Our 5 and 9-GHz detections show that it is feasible to monitor some MSPs at these observing frequencies, which are higher than those typically employed for long-term monitoring projects (350–3100 MHz; e.g. Desvignes et al., submitted; Manchester et al. 2013; Arzoumanian et al. 2015; Shannon et al. 2015). It is important to note that observing campaigns will only benefit from high-frequency detections of pulsars that are sufficiently bright to be able to take advantage of the reduced ISM effects. See § 5.2 for a more detailed discussion.

## 5 DISCUSSION

The new PSRIX data set already contains roughly monthly observations of 47 MSPs, black widow pulsars and relativistic binaries at 1.4 and 2.6 GHz spanning at least two years, including the 33 pulsars summarised in Tables 2 and 3. This data set is the successor of the venerable EBPP data set, and includes stronger detections and more precise TOAs thanks to the larger bandwidth and more robust design of PSRIX.

### 5.1 Improved Sensitivity to a GW Background

One of the primary goals of our monthly observations with PSRIX is to contribute to the EPTA and IPTA objective of detecting the GWB. To this end, we will be combining our observations with the EPTA and IPTA data sets.

We have estimated the improvement to GWB sensitivity made possible by switching from the EBPP to PSRIX for two separate scenarios: first, assuming all pulsars exhibit only pure white noise (e.g. radiometer noise or from pulse jitter), and second, assuming the pulsars also suffer from

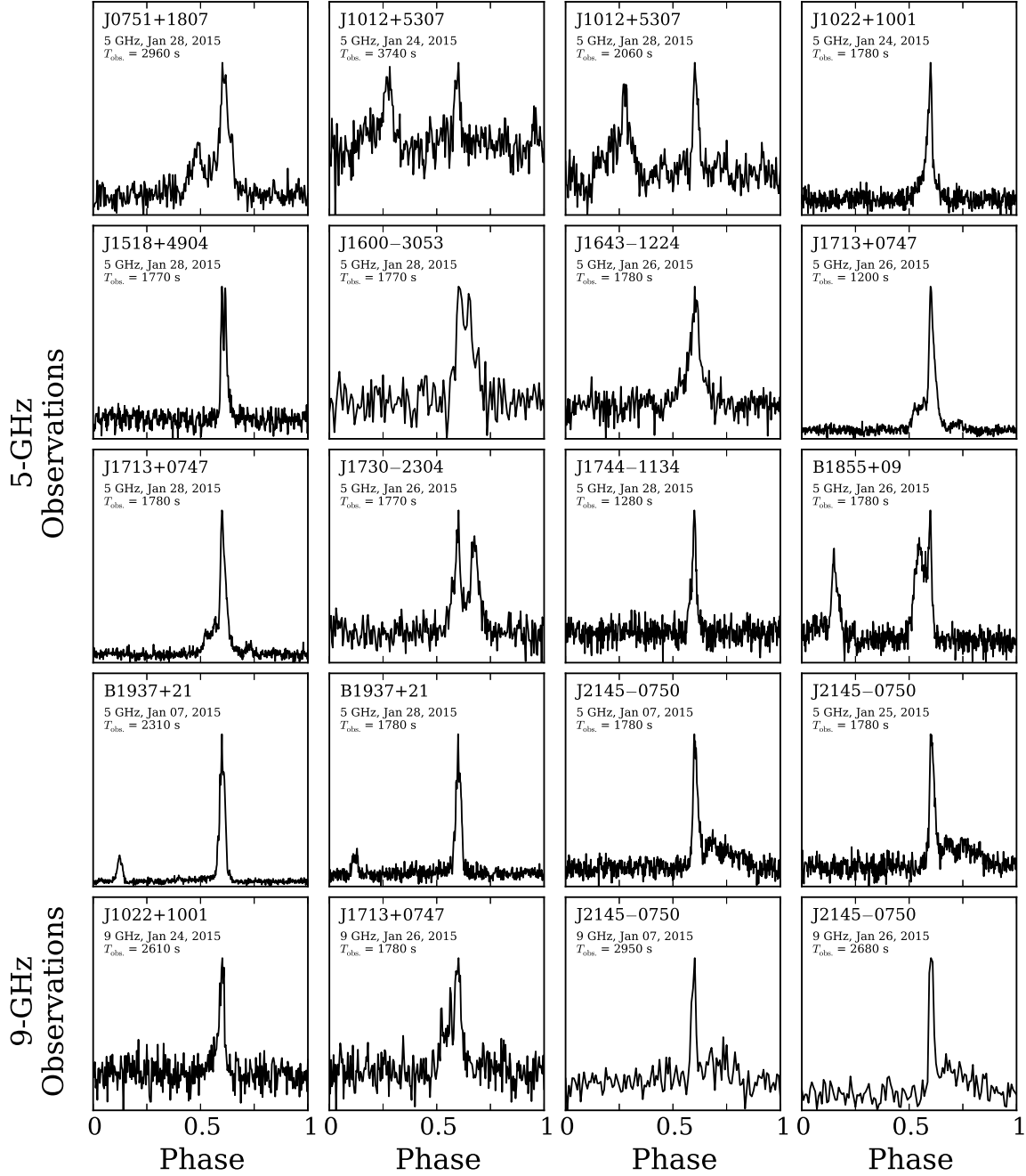


**Figure 5.** Integrated pulse profiles from PSRIX observations at 5 and 9-GHz. In all cases, a bandwidth of 500 MHz was used. These detections were cleaned of RFI and polarisation calibrated. See Table 4 for observation details.

red noise following a power-law spectrum (e.g. from intrinsic spin noise or uncorrected DM variations). In both cases, we considered a 7-pulsar<sup>12</sup> hybrid data set that combines the higher timing precision of the PSRIX TOAs with the longevity of the existing EBPP data set. We then compared our results for this hybrid data set to a hypothetical extension of the current EBPP data set without having switched to PSRIX.

In our first set of estimates, we assumed pulsars with pure white noise timing residuals. We assumed the timing residuals RMS in EBPP data is  $\text{RMS}_E = 1 \mu\text{s}$ , and the RMS of PSRIX residuals is improved by a factor  $\eta$  (i.e.  $\text{RMS}_P = \text{RMS}_E/\eta$ ). We performed separate estimates for  $\eta = 2, 3$ , and 5. For simplicity, we also assumed that the phase offset between the EBPP-era data and the PSRIX-era data is perfectly determined. We then used the Cramér-Rao Bound (e.g. Fisz 1963) to compute the minimum GWB amplitude required to reject the null hypothesis, which was that there is no GWB (i.e. a zero-amplitude GWB) at the  $1 \sigma$  level. A more complete description of the use of the Cramér-Rao Bound in the context of estimating PTA sensitivity to the GWB can be found in Caballero et al. (2015). In making our estimates, we assumed that the GWB signal has a power-law strain spectrum with an index of  $-2/3$ , appropriate for an isotropic stochastic background of super-massive black hole binaries. Improvement factors were determined by comparing the GWB amplitude derived for the hybrid data set with the analogous value computed for the pure EBPP-style data set. Our estimated improvement factors for  $\eta = 2, 3$ , and 5 as a function of date are shown in Fig. 6.

Our second set of estimates are determined following the same procedure described above, but assuming an additional red noise contribution to the timing residuals. We used a red noise spectrum with an amplitude corresponding to  $\text{RMS}_{\text{red}} = 100 \text{ ns}$  and a spectral index of  $\alpha_{\text{red}} = -1.5$  for all pulsars. This optimistically flat value of  $\alpha$  is within the measured range for MSPs,  $-7 \lesssim \alpha \lesssim -1$  (e.g. Arzoumanian et al. 2015; Caballero et al. 2015).<sup>13</sup> Even when assuming this nearly best-case red noise spectrum, we find the overall improvement in sensitivity to the GWB is considerably reduced. This is because only the power of the white noise is reduced by switching to PSRIX. It is, therefore, the red noise restricts the sensitivity to the GWB. We also find that the improvement factor saturates earlier because the low frequencies probed as the data set is extended are dominated by red noise. Thus, in the red-noise case, these lowest frequencies contribute little sensitivity to the GWB. The improvement factors for GWB sensitivity found for these red noise cases are indicated with the red curves in Fig. 6.

The difference between the black and red curves in Fig. 6 is caused by the presence of red noise, which can arise from a variety of sources (see e.g. Cordes & Shannon

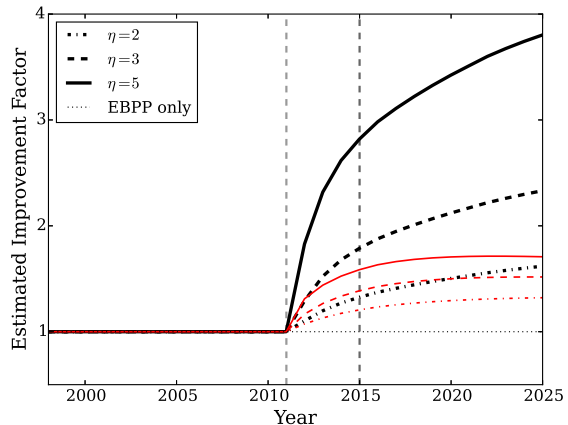


**Figure 6.** Estimated improvement in sensitivity to the GWB as a function of date provided by including PSRIX data compared to a hypothetical extended EBPP-only data set. We have assumed white noise with  $\text{RMS}_E = 1 \mu\text{s}$  for EBPP-era data (1997 to 2011), and  $\text{RMS}_P = \text{RMS}_E/\eta$  for PSRIX data. The baseline of our comparison assumed EBPP data only. By using the Cramér-Rao Bound we calculated the GWB amplitude at which the data would show a  $1 \sigma$  inconsistency with the no-GWB null hypothesis. The three black curves correspond to pure white noise and improvement factors of  $\eta = 2, 3$ , and 5. The red curves include an additional source of red noise with an amplitude corresponding to  $\text{RMS}_{\text{red}} = 100 \text{ ns}$  and a conservatively flat spectral index of  $\alpha_{\text{red}} = -1.5$  for all pulsars. See text for additional discussion.

2010). While it may not be possible to fully remove the deleterious effect of red noise from pulsar timing data, some of these noise processes (e.g. from the ISM – see § 5.2) can be mitigated, further improving the prospects for the detection of the GWB.

As suggested by Siemens et al. (2013), another way to counter the loss of sensitivity to the GWB due to pulsars’ red timing noise is to include other, possibly newly discovered MSPs in PTAs. This exemplifies the importance of ongoing high time and frequency radio pulsar surveys such as the Pulsar Arecibo L-Band Feed Array (PALFA) survey (Lazarus et al. 2015), the High-Time Resolution Universe (HTRU) surveys (Keith et al. 2010; Barr et al. 2013), and the Greenbank North Celestial Cap (GBNCC) survey (Stovall et al. 2014).

## 5.2 PTA Monitoring of MSPs at High Frequencies

ISM variations, primarily DM variations, can introduce a significant amount of red noise into the timing residuals of some MSPs (e.g. Lentati et al., in prep.; Cordes & Shannon 2010; Keith et al. 2013; Lee et al. 2014). This can be a major hindrance to reliably detecting long-timescale signals in the data (e.g. the nHz GWB spectrum being searched for with PTAs). Thus, mitigating ISM variations is of great importance. In general, this can be accomplished in two ways: 1) by avoiding ISM variations, either by discarding data sets contaminated by ISM variations or by observing at frequencies high enough that the amplitude of ISM-induced noise is sufficiently small (e.g. as was done by Shannon et al. 2015), and 2) by removing the ISM effects, either by leverag-

<sup>12</sup> We used the positions of PSRs J0218+4232, J0613–0200, J1022+1001, J1600–3053, J1713+0747, B1855+09, and J2145–0750. Because we are computing improvement factors, we find there is no significant difference in the results as the number of pulsars is increased.

<sup>13</sup> MSPs with very steep spectral indices (e.g. B1937+21) are not typically used in searches for the GWB.

ing multi-frequency and wide-band observations to measure DM variations (e.g. Keith et al. 2013; Demorest et al. 2013; Arzoumanian et al. 2015).

The effect of the ISM diminishes with increasing observing frequency: DM delays scale as  $\tau_d \propto f^{-2}$  (e.g. Lorimer & Kramer 2004) and pulse broadening caused by interstellar scattering scales as  $\tau_s \propto f^{-3.86 \pm 0.16}$  (Bhat et al. 2004). Therefore, pulsar timing data from high-frequency observations will contain less significant red ISM noise. Unfortunately, the radio spectra of pulsars, which are generally described by a simple power law,  $S \propto f^\alpha$ , are rather steep, with spectral indices of  $-1 \lesssim \alpha \lesssim -2$  (Maron et al. 2000; Bates et al. 2013), making it difficult to completely avoid ISM variations while maintaining the  $S/N$  required for high-precision timing. Thus, in practice, ISM effects cannot be completely ignored by observing at arbitrarily high frequencies. Some effort to remove these effects is necessary.

When removing DM variations the key resulting quantity is the infinite-frequency TOA,  $T_\infty$  (i.e. the DM-corrected TOA). Estimates of  $T_\infty$  can be made by combining multi-frequency observations or by splitting a single wide-band observation into multiple sub-bands (see e.g. Lee et al. 2014). The uncertainty on  $T_\infty$  is  $\sigma_\infty = \sqrt{\langle \delta T_\infty^2 \rangle}$ , and in the two-band case, is given by (Eq. 12 of Lee et al. 2014)

$$\langle \delta T_\infty^2 \rangle = \frac{f_1^4 \sigma_1^2 + f_2^4 \sigma_2^2}{(f_1^2 - f_2^2)^2}, \quad (2)$$

where the  $f_i$  and  $\sigma_i$  terms are the centre frequencies and TOA uncertainties of the two bands, respectively.

To measure and remove DM variations, timing data at 1 to 3 GHz are typically complemented by low-frequency observations (e.g.  $\lesssim 350$  MHz). To illustrate the precision on  $T_\infty$  attainable, we have estimated the relative improvement in  $\sigma_\infty$  from combining observations with the LOFAR international station at Effelsberg,<sup>14</sup> with PSRIX data at 1.4 GHz to compute. Note that we have neglected the differences in propagation paths through Galaxy of the lower and high-frequency radio emission due to scattering (see Cordes et al. 2015, for a discussion of this effect). We estimated the ratio of TOA uncertainties derived from observations of the same duration with different observing systems, ‘‘A’’ and ‘‘B’’, using

$$\begin{aligned} \frac{\sigma_{t_A}}{\sigma_{t_B}} &= \frac{(S/N)_B}{(S/N)_A} \\ &= \frac{S_{\text{sys},A}}{S_{\text{sys},B}} \sqrt{\frac{\Delta f_A}{\Delta f_B}} \left( \frac{f_{\text{hi},B}^{(\alpha+1)} - f_{\text{lo},B}^{(\alpha+1)}}{f_{\text{hi},A}^{(\alpha+1)} - f_{\text{lo},A}^{(\alpha+1)}} \right), \quad (3) \end{aligned}$$

where  $S_{\text{sys}}$  is the system-equivalent flux density,  $\Delta f$  is the recorded bandwidth,  $f_{\text{lo}}$  and  $f_{\text{hi}}$  are the low and high frequency edges of the recorded band, respectively, and  $\alpha$  is the spectral index. In deriving Eq. 3, we have ignored the effect of profile evolution across the band, which is minimal for MSPs (Kramer et al. 1999), as well as pulse broadening, which can be significant at 150 MHz. We have also assumed that  $S_{\text{sys}}$  is constant across the individual bands. Our estimates are plotted in Fig. 7 for  $-3 \leq \alpha \leq -1$ .

For simplicity, in Fig. 7 we have assumed the entire

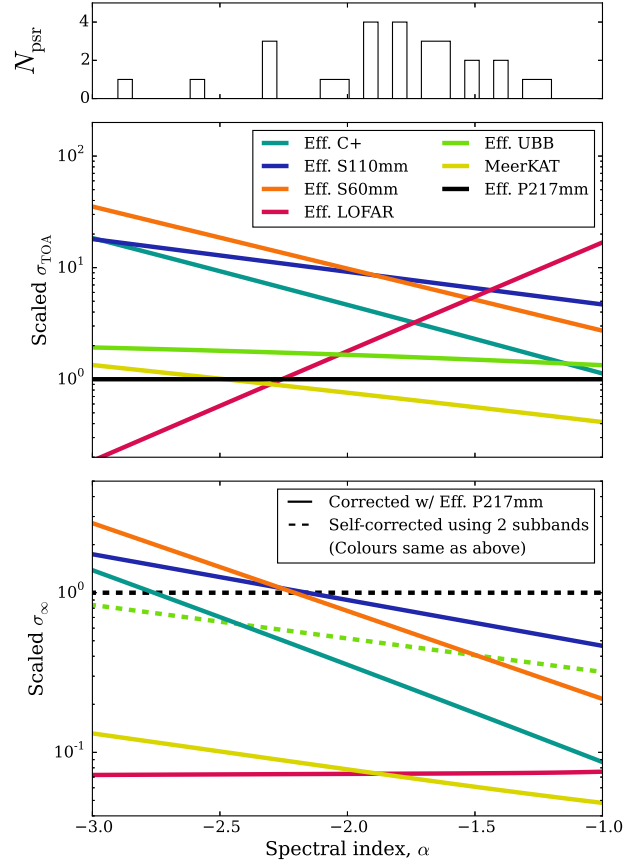


**Figure 7.** *Top* – Distribution of spectral indices from the ATNF Pulsar Catalogue for the pulsars in Table 2.

*Middle* – TOA uncertainties for various existing and future observing systems scaled to what is achievable with PSRIX using the P217mm receiver as a function of pulsar radio spectral index. Lower values indicate more precise (i.e. better) TOAs. Note that the estimated TOA precision of the UBB receiver is worse than the P217mm receiver because of the former’s high SEFD, which will be reduced when a high-pass filter is installed.

*Bottom* – The uncertainty of the infinite frequency TOA (i.e. the uncertainty of the DM-corrected TOA),  $\sigma_\infty$ , obtained from combining Effelsberg 1.4-GHz (P217mm) detections with data from another observing system relative to the uncertainty of the self-corrected P217mm observation. The  $\sigma_\infty$  values for the self-corrected observations are estimated assuming the band is divided evenly into two parts. Note, that doubling the integration time only improves  $\sigma_\infty$  by  $\sqrt{2}$ .

recorded bandwidth is summed to form a single TOA. This is a reasonable assumption given recent work on wide-band template matching (Pennucci et al. 2014; Liu et al. 2014). In fact, by using these new wide-band TOA determination algorithms it is possible to simultaneously account for profile evolution, DM variations, scattering, and scintillation while summarising wide-band observations into a single TOA.

Clearly, complementing PSRIX TOAs with observations using the Effelsberg LOFAR station, provides precise DM-corrected TOAs. However, there are some complications with using low-frequency data to remove DM varia-

<sup>14</sup> The international LOFAR station at Effelsberg is also known as ‘‘DE601’’.

tions. First, the background of Galactic synchrotron emission is strong and line-of-sight dependent (Haslam et al. 1982). Thus, MSPs in unfortunate directions may be too weak to use low-frequency observations to make DM measurements. Another possible complication, not included in our estimates, is spectral turnover, which occurs in a significant fraction of MSPs (Kuniyoshi et al. 2015). This also conspires to weaken detections at low frequencies. Finally, there is concern that the DMs measured at low frequencies are different than those measured at higher frequencies due to differences in the ISM probed as a result of interstellar scattering (Cordes et al. 2015).

Our 5 and 9-GHz detections of several MSPs indicate that complementing timing campaigns at 1 to 3 GHz with observations at higher frequencies might be a viable alternative for mitigating ISM effects. Fig. 7 includes estimates of  $\sigma_\infty$  attainable by complementing 1.4 GHz PSRIX data with observations from current and planned receiver systems. Using the current 5-GHz set-up with PSRIX should provide better TOA precision than the 2.6-GHz set-up described in § 2 for  $\alpha \gtrsim -1.9$ , as well as better  $\sigma_\infty$  for  $\alpha \gtrsim -2.25$ , thanks to the larger frequency separation between the bands.

We also examined new wide-bandwidth receivers coming online, such as the 0.6-to-2.7-GHz UBB receiver at Effelsberg,<sup>15</sup> as well as the new 4-to-9-GHz “C+” receiver currently being commissioned at Effelsberg, and the 1.8-to-3.5-GHz receivers being designed at the MPIfR for MeerKAT. The assumed receiver parameters are shown Table 5.

Effelsberg’s C+ receiver and the MeerKAT 1.8-to-3.5-GHz observing systems present significant improvements in the bandwidths currently available for pulsar timing at these frequencies, and thus provide compelling cases for using high-frequency observations to mitigate ISM-related noise. Furthermore, other sensitive high-frequency observing systems (e.g. the 3.85–6 GHz “C-band” receiver at the Arecibo Observatory, the 2–4 GHz “S-band” system at the Jansky Very Large Array (JVLA), and the 4–8 GHz “C-band” system at the JVLA) should be considered for regular PTA monitoring of MSPs. Furthermore, the potential high-frequency capabilities of the SKA could also be important for PTA-studies.

Note that, at  $\sim 5$  GHz we expect slow, roughly hourly, intensity variations of only  $\sim 10$  to 30%. Also, the attenuation of the transmission of radio waves through the atmosphere due to water vapour only becomes a concern at  $f \gtrsim 10$  GHz.

When formulating observing strategies for high-precision, multi-frequency timing campaigns, deciding what observing systems to use should depend on the spectral index of the pulsar, the magnitude of the noise introduced by ISM effects, and the shape of the pulse profile, including the degree of profile broadening. Furthermore, deciding how often multi-frequency observations are necessary for a particular pulsar depends on the timescale of the DM variations affecting the pulsar (see e.g. Keith et al. 2013). At Effelsberg, because the secondary-focus receivers are always

available, and can be switched-to within minutes, issues arising from the non-simultaneity of multi-frequency observations described by Lam et al. (2015) are not a concern, as they may be at other telescopes.

## 6 CONCLUSIONS

We have described how the PSRIX backend is being used at the Effelsberg radio telescope for monthly EPTA observations. The coherently dedispersed data from PSRIX have a larger bandwidth than what is possible with its predecessor, the EBPP. As a result, the now four-year-old PSRIX data set has stronger detections, more precise TOAs, and will improve the sensitivity to the GWB compared to the EBPP data.

We have also shown how bright, highly stable MSPs being monitored by the EPTA can be detected at 5 and 9 GHz. Given the reduced ISM effects at these frequencies compared to 1.4 GHz and the ability to more precisely correct DM variations, there could be advantages to complementing existing data sets (typically  $1 \lesssim f \lesssim 3$  GHz) with observations at these higher frequencies. This is especially true considering the new wide-bandwidth, high-frequency receivers currently being commissioned, and those expected to come online in the next few years.

We would like to thank Cees Bassa and Jason Hessels for helping to conceive and develop TOASTER. We would also like to thank Paulo Freire and Gregory Desvignes for useful discussions, as well as Stefan Osłowski, Golam Shaifullah, Antoine Lassus, and John Antoniadis for helping to observe. PL and EG acknowledge support from IMPRS Bonn/Cologne. RNC acknowledges the support of IMPRS Bonn/Cologne and the Bonn-Cologne Graduate School. KJL gratefully acknowledges support from National Basic Research Program of China, 973 Program, 2015CB857101 and NSFC 11373011. The PSRIX backend was constructed as part of the LEAP project, which was funded by the ERC Advanced Grant LEAP, Grant Agreement Number 227947 (PI M. Kramer).

## REFERENCES

- Antoniadis, J., Freire, P. C. C., Wex, N., et al. 2013, *Science*, 340, 448
- Arzoumanian, Z., Brazier, A., Burke-Spolaor, S., et al. 2015, *ArXiv e-prints*, arXiv:1505.07540
- Backer, D. C., Dexter, M. R., Zepka, A., et al. 1997, *PASP*, 109, 61
- Barr, E. D., Champion, D. J., Kramer, M., et al. 2013, *MNRAS*, 435, 2234
- Bassa, C. G., Janssen, G. H., Karuppusamy, R., et al. 2015, *ArXiv e-prints*, arXiv:1511.06597
- Bates, S. D., Lorimer, D. R., & Verbiest, J. P. W. 2013, *MNRAS*, 431, 1352
- Berkhuijsen, E. M., & Müller, P. 2008, *A&A*, 490, 179
- Bhat, N. D. R., Cordes, J. M., Camilo, F., Nice, D. J., & Lorimer, D. R. 2004, *ApJ*, 605, 759
- Bhat, N. D. R., Gupta, Y., & Rao, A. P. 1998, *ApJ*, 500, 262
- Britton, M. C. 2000, *ApJ*, 532, 1240

<sup>15</sup> Currently, the UBB receiver at Effelsberg can observe frequencies as low as 0.6 GHz. However, since the RFI is particularly strong below 1 GHz, a high-pass filter will be installed around 1.1 GHz to improve the overall performance of the receiver.

- Caballero, R. N., Lee, K. J., Lentati, L., et al. 2015, ArXiv e-prints, arXiv:1510.09194
- Cognard, I., Guillemot, L., Johnson, T. J., et al. 2011, *ApJ*, 732, 47
- Cordes, J. M., & Shannon, R. M. 2010, ArXiv e-prints, arXiv:1010.3785
- Cordes, J. M., Shannon, R. M., & Stinebring, D. R. 2015, ArXiv e-prints, arXiv:1503.08491
- Demorest, P. B., Pennucci, T., Ransom, S. M., Roberts, M. S. E., & Hessels, J. W. T. 2010, *Nat.*, 467, 1081
- Demorest, P. B., Ferdman, R. D., Gonzalez, M. E., et al. 2013, *ApJ*, 762, 94
- Dolch, T., Lam, M. T., Cordes, J., et al. 2014, *ApJ*, 794, 21
- Eatough, R. P., Falcke, H., Karuppusamy, R., et al. 2013, *Nat.*, 501, 391
- Fisz, M. 1963, *Probability theory and mathematical statistics (Polish Scientific)*
- Ford, J. M., Demorest, P., & Ransom, S. 2010, in *Society of Photo-Optical Instrumentation Engineers (SPIE) Conference Series*, Vol. 7740, Society of Photo-Optical Instrumentation Engineers (SPIE) Conference Series, 0
- Freire, P. C. C., Bassa, C. G., Wex, N., et al. 2011, *MNRAS*, 412, 2763
- Haslam, C. G. T., Salter, C. J., Stoffel, H., & Wilson, W. E. 1982, *A&A Supp.*, 47, 1
- Hobbs, G. B., Edwards, R. T., & Manchester, R. N. 2006, *MNRAS*, 369, 655
- Hotan, A. W., van Straten, W., & Manchester, R. N. 2004, *PASA*, 21, 302
- Jacoby, B. A., Bailes, M., Ord, S. M., Knight, H. S., & Hotan, A. W. 2007, *ApJ*, 656, 408
- Janssen, G. H., Stappers, B. W., Bassa, C. G., et al. 2010, *A&A*, 514, A74
- Janssen, G. H., Stappers, B. W., Kramer, M., et al. 2008, *A&A*, 490, 753
- Keith, M. J., Jameson, A., van Straten, W., et al. 2010, *MNRAS*, 409, 619
- Keith, M. J., Coles, W., Shannon, R. M., et al. 2013, *MNRAS*, 429, 2161
- Kondratiev, V. I., Verbiest, J. P. W., Hessels, J. W. T., et al. 2015, ArXiv e-prints, arXiv:1508.02948
- Kramer, M., Lange, C., Lorimer, D. R., et al. 1999, *ApJ*, 526, 957
- Kramer, M., Xilouris, K. M., Lorimer, D. R., et al. 1998, *ApJ*, 501, 270
- Kramer, M., Stairs, I. H., Manchester, R. N., et al. 2006, *Science*, 314, 97
- Kuniyoshi, M., Verbiest, J. P. W., Lee, K. J., et al. 2015, ArXiv e-prints, arXiv:1507.03732
- Lam, M. T., Cordes, J. M., Chatterjee, S., & Dolch, T. 2015, *ApJ*, 801, 130
- Lazaridis, K., Wex, N., Jessner, A., et al. 2009, *MNRAS*, 400, 805
- Lazaridis, K., Verbiest, J. P. W., Tauris, T. M., et al. 2011, *MNRAS*, 414, 3134
- Lazarus, P., Brazier, A., Hessels, J. W. T., et al. 2015, *ApJ*, 812, 81
- Lee, K. J., Bassa, C. G., Janssen, G. H., et al. 2014, *MNRAS*, 441, 2831
- Lentati, L., Alexander, P., Hobson, M. P., et al. 2014, *MNRAS*, 437, 3004
- Lentati, L., Taylor, S. R., Mingarelli, C. M. F., et al. 2015, ArXiv e-prints, arXiv:1504.03692
- Liu, K., Desvignes, G., Cognard, I., et al. 2014, *MNRAS*, 443, 3752
- Lommen, A. N., Zepka, A., Backer, D. C., et al. 2000, *ApJ*, 545, 1007
- Lorimer, D. R., & Kramer, M. 2004, *Handbook of Pulsar Astronomy*, ed. R. Ellis, J. Huchra, S. Kahn, G. Rieke, & P. B. Stetson
- Lorimer, D. R., Faulkner, A. J., Lyne, A. G., et al. 2006, *MNRAS*, 372, 777
- Lynch, R. S., Boyles, J., Ransom, S. M., et al. 2013, *ApJ*, 763, 81
- Manchester, R. N., Hobbs, G., Bailes, M., et al. 2013, *PASA*, 30, 17
- Maron, O., Kijak, J., Kramer, M., & Wielebinski, R. 2000, *A&A Supp.*, 147, 195
- Ng, C., Bailes, M., Bates, S. D., et al. 2014, *MNRAS*, 439, 1865
- Pennucci, T. T., Demorest, P. B., & Ransom, S. M. 2014, *ApJ*, 790, 93
- Sanidas, S. A., Battye, R. A., & Stappers, B. W. 2012, *Phys. Rev. D*, 85, 122003
- Sesana, A. 2013, *Classical and Quantum Gravity*, 30, 224014
- Shannon, R. M., Ravi, V., Lentati, L. T., et al. 2015, *Science*, 349, 1522
- Shao, L., Caballero, R. N., Kramer, M., et al. 2013, *Classical and Quantum Gravity*, 30, 165019
- Siemens, X., Ellis, J., Jenet, F., & Romano, J. D. 2013, *Classical and Quantum Gravity*, 30, 224015
- Stairs, I. H., Faulkner, A. J., Lyne, A. G., et al. 2005, *ApJ*, 632, 1060
- Stovall, K., Lynch, R. S., Ransom, S. M., et al. 2014, *ApJ*, 791, 67
- van Haarlem, M. P., Wise, M. W., Gunst, A. W., et al. 2013, *A&A*, 556, A2
- Will, C. M. 1993, *Theory and Experiment in Gravitational Physics*

**Table 1.** Observing Set-Ups Used

Parameter	Receiver				
	P200mm	P217mm (Central beam)	S110mm	S60mm	S36mm
Receiver band (MHz)	1290 – 1430	1240 – 1480	2599.5 – 2679.5	4600 – 5100	7900 – 9000
System Temperature (K)	21, 27 <sup>a</sup>	23	17	27	22
Gain (K/Jy)	1.55	1.37	1.5	1.55	1.35
Recorded band (MHz)	1247.5 – 1447.5	1247.5 – 1447.5	2527 – 2727	4607.8 – 5107.8	8107.8 – 8607.8
Usable bandwidth (MHz)	140	200	80	500	500
Number of sub-bands	8	8	8	32	32

NOTES. — All of these receivers have circularly polarised feeds. Also, in all cases 1024 phase bins were recorded across each pulse profile.

<sup>a</sup> The reported temperatures for the two polarisation channels.

**Table 2.** Summary of monthly monitoring observations of EPTA pulsars at 1.4 GHz

Pulsar	Period (ms)	DM (pc cm <sup>-3</sup> )	Obs. Span (YYYY/MM)	$N_{\text{obs.}}$	$N_{\text{det.}}$	$N_{\text{cal.}}$	$\langle S/N \rangle^a$	$\langle S \rangle^b$ (mJy)	$S_{\text{med.}}$ (mJy)	$S_{\text{pub.}}^c$ (mJy)	Ref. <sup>d</sup>
J0023+0923	3.05	14.3	2012/03 – 2014/10	37	32	13	32	0.57(9)	0.47	–	–
J0030+0451	4.87	4.3	2011/05 – 2015/02	46	46	11	48	1.20(16)	1.08	0.6(2)	(1)
J0218+4232	2.32	61.3	2011/04 – 2015/02	48	48	11	61	0.97(6)	1.01	0.9(2)	(2)
J0340+4129	3.30	49.6	2011/04 – 2015/02	44	44	10	34	0.45(4)	0.43	–	–
J0348+0432	39.12	40.5	2011/07 – 2015/04	354	231	80	38	0.51(2)	0.48	–	–
J0613–0200	3.06	38.8	2011/03 – 2015/02	62	61	13	133	1.91(9)	1.87	2.3 <sup>e</sup>	(3)
J0621+1002	28.85	36.6	2011/03 – 2015/02	56	55	14	92	1.34(7)	1.31	1.9(3)	(2)
J0751+1807	3.48	30.2	2011/01 – 2015/02	89	81	23	106	1.07(7)	1.02	3.2(7)	(2)
J1012+5307	5.26	9.0	2011/03 – 2015/02	58	55	12	173	3.8(7)	3.3	3(1)	(2)
J1022+1001	16.45	10.3	2011/01 – 2015/02	119	114	16	308	2.3(8)	1.0	6.1 <sup>e</sup>	(3)
J1024–0719	5.16	6.5	2011/03 – 2015/02	60	57	15	113	2.1(5)	1.1	1.5 <sup>e</sup>	(3)
J1518+4904	40.93	11.6	2011/03 – 2014/10	226	190	149	379	2.5(2)	1.7	4(2)	(2)
J1600–3053	3.60	52.3	2011/03 – 2015/02	45	45	9	136	1.79(5)	1.78	2.5 <sup>e</sup>	(3)
J1640+2224	3.16	18.4	2011/03 – 2015/02	83	72	11	66	0.4(1)	0.3	2(1)	(2)
J1643–1224	4.62	62.4	2011/03 – 2015/02	47	47	13	276	4.2(1)	4.3	4.8 <sup>e</sup>	(3)
J1713+0747	4.57	16.0	2011/03 – 2015/02	105	96	21	746	4.9(1.6)	2.4	10.2 <sup>e</sup>	(3)
J1730–2304	8.12	9.6	2011/03 – 2015/02	50	48	10	239	5.1(1.4)	3.6	3.9 <sup>e</sup>	(3)
J1738+0333	5.85	33.8	2011/06 – 2015/02	37	36	7	44	0.52(5)	0.50	–	–
J1741+1351	3.75	24.0	2011/10 – 2015/02	38	36	9	29	0.50(6)	0.56	0.93 <sup>f</sup>	(4)
J1744–1134	4.07	3.1	2011/03 – 2014/12	49	48	10	193	1.9(6)	1.1	3.1 <sup>e</sup>	(3)
J1853+1303	4.09	30.6	2013/05 – 2015/02	20	18	7	34	0.6(1)	0.5	0.4(2)	(5)
B1855+09	5.36	13.3	2011/03 – 2015/02	47	45	10	177	3.6(8)	2.3	5.0 <sup>e</sup>	(3)
J1911+1347	4.63	31.0	2013/05 – 2015/02	22	21	7	57	0.87(15)	0.71	0.08 <sup>f</sup>	(6)
J1918–0642	7.65	26.6	2011/03 – 2015/02	45	45	10	67	1.5(3)	1.2	0.58(2) <sup>g</sup>	(7)
B1937+21	1.56	71.0	2011/03 – 2015/02	84	75	11	524	12(1)	12	13.2 <sup>e</sup>	(3)
J2010–1323	5.22	22.2	2012/09 – 2015/02	25	24	8	70	0.64(7)	0.58	1.6 <sup>f</sup>	(4)
J2017+0603	2.90	23.9	2011/04 – 2015/02	44	36	10	25	0.48(9)	0.40	0.5(2)	(8)
J2043+1711	2.38	20.7	2011/04 – 2015/02	44	19	7	15	0.246(16)	0.237	–	–
J2145–0750	16.05	9.0	2011/03 – 2015/02	52	50	10	382	2.9(5)	2.6	8.9 <sup>e</sup>	(3)
J2229+2643	2.98	23.0	2011/03 – 2015/02	48	40	9	98	0.5(1)	0.5	0.9(2)	(2)
J2234+0944	3.63	17.8	2011/11 – 2014/10	42	39	15	62	0.94(14)	0.93	–	–
J2317+1439	3.45	21.9	2011/03 – 2015/02	52	46	11	54	0.8(3)	0.3	4(1)	(2)
J2322+2057	4.81	13.4	2013/07 – 2015/02	21	17	6	20	0.5(2)	0.3	–	–

<sup>a</sup> Mean  $S/N$ , computed using  $S/N$  values only from observations longer than 20 minutes and scaled to a canonical integration time of 30 minutes.

<sup>b</sup> Mean phase-averaged flux density. The uncertainty reported is the standard error on the mean (i.e.  $\sigma_{S_{\text{mean}}}/\sqrt{N_{\text{cal.}}}$ ).

<sup>c</sup> Previously published phase-averaged flux density.

<sup>d</sup> References for  $S_{\text{pub.}}$  – (1): Lommen et al. (2000), (2): Kramer et al. (1998), (3): Manchester et al. (2013), (4): Jacoby et al. (2007), (5): Stairs et al. (2005), (6): Lorimer et al. (2006), (7): Janssen et al. (2010), (8): Cognard et al. (2011)

<sup>e</sup> Manchester et al. (2013) report the RMS of multiple flux density measurements. This does not represent the uncertainty on the mean, but rather how much scintillation can modulate the observed flux density.

<sup>f</sup> No uncertainty reported.

<sup>g</sup> The flux density of PSR J1918–0642 reported by Janssen et al. (2010) is for a single observation. Thus, the value is likely affected by scintillation, but the uncertainty does not take scintillation into account.

**Table 3.** Summary of monthly monitoring observations of EPTA pulsars at 2.6 GHz

Pulsar	Period (ms)	DM (pc cm <sup>-3</sup> )	Obs. Span (YYYY/MM)	$N_{\text{obs.}}$	$N_{\text{det.}}$	$\langle S/N \rangle^a$
J0023+0923	3.05	14.3	2012/03 – 2014/10	28	3	14
J0030+0451	4.87	4.3	2011/05 – 2015/02	40	34	13
J0218+4232	2.32	61.3	2011/05 – 2015/02	17	0	–
J0340+4129	3.30	49.6	2011/05 – 2015/02	36	13	10
J0613–0200	3.06	38.8	2011/03 – 2015/02	42	37	20
J0621+1002	28.85	36.6	2011/03 – 2015/02	39	29	15
J0751+1807	3.48	30.2	2011/03 – 2015/02	49	35	30
J1012+5307	5.26	9.0	2011/03 – 2015/02	48	46	39
J1022+1001	16.45	10.3	2011/03 – 2015/02	60	54	109
J1024–0719	5.16	6.5	2011/05 – 2015/02	46	39	20
J1518+4904	40.93	11.6	2011/03 – 2014/06	7	6	63
J1600–3053	3.60	52.3	2011/05 – 2014/12	31	29	25
J1640+2224	3.16	18.4	2011/06 – 2015/02	48	32	13
J1643–1224	4.62	62.4	2011/05 – 2015/01	36	36	57
J1713+0747	4.57	16.0	2011/05 – 2015/02	46	44	258
J1730–2304	8.12	9.6	2011/05 – 2015/02	35	24	48
J1738+0333	5.85	33.8	2011/06 – 2015/01	9	2	32
J1741+1351	3.75	24.0	2012/01 – 2015/02	35	15	17
J1744–1134	4.07	3.1	2011/05 – 2015/01	39	37	27
J1853+1303	4.09	30.6	2013/05 – 2015/02	24	6	10
B1855+09	5.36	13.3	2011/03 – 2015/02	43	35	46
J1911+1347	4.63	31.0	2013/05 – 2015/02	22	17	14
J1918–0642	7.65	26.6	2011/05 – 2015/02	41	24	22
B1937+21	1.56	71.0	2011/03 – 2015/02	54	48	87
J2010–1323	5.22	22.2	2012/09 – 2015/02	26	18	17
J2017+0603	2.90	23.9	2011/07 – 2015/02	16	1	11
J2043+1711	2.38	20.7	2011/05 – 2015/02	17	1	6
J2145–0750	16.05	9.0	2011/03 – 2015/02	47	45	70
J2229+2643	2.98	23.0	2011/03 – 2015/02	46	35	25
J2234+0944	3.63	17.8	2011/11 – 2014/10	36	28	21
J2317+1439	3.45	21.9	2011/03 – 2015/02	43	28	14
J2322+2057	4.81	13.4	2013/07 – 2015/02	16	3	8

<sup>a</sup> Mean  $S/N$ , computed using  $S/N$  values only from observations longer than 20 minutes and scaled to a canonical integration time of 30 minutes.**Table 4.** High-frequency observations

Pulsar	Obs. Start (UTC)	Integration Time (s)	$S/N$	Flux Density (mJy)	TOA Uncertainty ( $\mu\text{s}$ )
<i>5-GHz Observations</i>					
J0751+1807	2015-Jan-28 02:12:19	2960	47.05	0.375	2.890
J1012+5307	2015-Jan-24 20:03:30 <sup>a</sup>	3740	15.96	0.209	7.278
	2015-Jan-28 03:11:00	2060	26.22	0.385	4.866
J1022+1001	2015-Jan-24 21:01:09	1780	39.47	0.562	3.552
J1518+4904	2015-Jan-28 03:59:29	1770	25.51	0.441	5.87
J1600–3053	2015-Jan-28 06:38:40	1770	10.49	0.318	6.657
J1643–1224	2015-Jan-26 07:14:40	1780	22.78	0.343	4.920
J1713+0747	2015-Jan-26 06:13:59	1200	133.87	1.463	0.470
	2015-Jan-28 04:38:09	1780	110.45	1.102	0.541
J1730–2304	2015-Jan-26 07:51:49	1770	27.10	0.503	5.892
J1744–1134	2015-Jan-28 06:09:40	1280	14.40	0.389	1.421
B1855+09	2015-Jan-26 08:29:29	1780	52.50	0.895	1.482
B1937+21	2015-Jan-07 15:13:19	2310	86.56	1.234	0.101
	2015-Jan-28 05:26:40	1780	35.91	0.639	0.211
J2145–0750	2015-Jan-07 15:59:59	1780	52.70	0.702	3.812
	2015-Jan-25 15:20:19	1780	54.00	0.797	3.883
<i>9-GHz observations</i>					
J1022+1001	2015-Jan-24 22:09:30	2610	10.06	0.233	18.237
J1713+0747	2015-Jan-26 06:38:40	1780	15.74	0.258	5.297
J2145–0750	2015-Jan-07 17:11:10	2950	16.90	0.251	12.269
	2015-Jan-26 13:37:39	2680	16.43	0.218	10.631

<sup>a</sup> Two closely spaced observations added together.

**Table 5.** Parameters for selected available and planned observing set-ups

	Observing Set-Up			
	Effelsberg	Effelsberg	MeerKAT	LOFAR
Telescope	Effelsberg	Effelsberg	MeerKAT	LOFAR
Receiver	UBB	S45mm (“C+”)	S-band	DE601 <sup>a</sup>
Receiver band (MHz)	600 – 2700 <sup>b</sup>	4000 – 9300	1600 – 3500	111.5 – 186.5
Recorded band (MHz)	1100 – 2700	4000 – 6000	1600 – 2300	111.5 – 186.5
System Temperature (K)	25/(55) <sup>c</sup>	~25 <sup>d</sup>	<25 <sup>e</sup>	– <sup>f</sup>
Gain (K/Jy)	1.25	~1.35 <sup>d</sup>	2.5	– <sup>f</sup>
SEFD (Jy)	45	18.5	10	1500 <sup>f</sup>

<sup>a</sup> DE601 is the international LOFAR station located at Effelsberg.

<sup>b</sup> The observing band of the UBB receiver currently goes as low as 600 MHz. However, strong interference from digital television broadcasts at ~500 to 800 MHz and GSM emission at ~900 MHz greatly deteriorates the quality of the observations. There are plans to insert a high-pass filter at ~1100 MHz. We use this planned low-frequency band for our estimates.

<sup>c</sup> The strong interference in the UBB band causes the system temperature to be on the order of ~55 K, significantly higher than the value of  $T_{\text{sys}} = 25$  K measured in the lab. A high-pass filter will be installed around 1100 MHz and should lower  $T_{\text{sys}}$  to ~25 K. Nevertheless, in our estimates of the system performance, we use the current, higher, measured value to be conservative.

<sup>d</sup> Preliminary estimate.

<sup>e</sup> This is the target system temperature. In our estimates we use  $T_{\text{sys}} = 25$  K.

<sup>f</sup> We estimated the SEFD Effelsberg LOFAR station by scaling the SEFD of the LOFAR core published by van Haarlem et al. (2013).